Design and Investigation of Tunable Gyrator Resonance Circuit Implemented on AMS 0.35µm Process

IVAN UZUNOV
Smartcom Bulgaria AD
Sofia
BULGARIA

ATANAS TANEV

MARIN HRISTOV
Department of Microelectronics, Faculty of Electronic Engineering and Technologies
Technical University of Sofia
Sofia
BULGARIA
ivan_uzunov@smartcom.bg; atanev@ecad.tu-sofia.bg; mhristov@ecad.tu-sofia.bg

Abstract: — The paper considers some basic problems in the design of tunable fully differential gyrator resonance circuit. First is presented briefly the theory of the parallel gyrator tank with emphasizing on the effects from the amplifier imperfections. Then is considered the design of a single stage operational transconductance amplifier (OTA) with source degeneration for better linearity. It is demonstrated by simulation that wide range of variation of OTA's g_m with preserving the linearity can be achieved by using of an architecture, consisting of several parallel connected differential cells with different g_ms. They are switched on and off and the designed amplifier has 3 cells with g_m of 50, 100 and 200µS. The resonance frequency of the gyrator tank, created with two such amplifiers, can be increased 7 times. The Q-factor of the tank is also tunable by negative resistances in parallel to the OTA outputs.

Key-Words: - active filters, gyrator, programmable filters; operational transconductance amplifiers, CMOS, nonlinear distortion.

1 Introduction

Probably the most often used analog integrated filters nowadays are the Gm-C filters, consisting of operational transconductance amplifiers (OTA), capacitors and rarely resistors [1,2]. Their major advantage, compared with the other classes of analog filters, is the extremely wide frequency area, in which they can be implemented. This range is determined from downside by the opportunity to design OTAs with very small g_m (pole frequencies of these filters are defined by the ratio g_m/C of some elements). The limitation for the upper side comes from the higher frequency of operation of the amplifiers. Since the required g_m is not very high, OTA can work at much higher frequencies compared with the standard voltage operational amplifiers. There are examples of filters operating in the range of few Hz [3] and even below 1 Hz [4] and in the same time there are Gm-C filters intended for GHz range [5].

Another important advantage of Gm-C filters is their tunability. The pole frequencies can be controlled by OTAs g_m or by the capacitors. Different ways are applied for varying of the transconductances and first of them is by changing the dc currents in some of amplifier stages [1], [6]-[10]. Other methods for g_m control are existing too: by changing of the degeneration resistors in the sources of the amplifying transistors, used also for improving the linearity [11],[12]; by connecting of several Gm-cells in parallel, which can be digitally switched on and off [13],[14]; by connecting of switchable transistors in parallel or in series in order to control their W and L [14]; etc. The other tuning method, by changing the capacitors, is used also but rarely (examples are given in [11],[15]). Both methods are compared in [16] and there is proved that the changing of the capacitors for tuning the filter has a drawback – the filter dynamic range also changes.

Pole Q-factors is also necessary to be tuned. This tuning is applied basically in biquads and in filters, consisting of cascaded biquads.

Usually the tuning is applied for compensation the inaccuracies due to process, voltage and temperature (PVT) variations or for creating of tracking filters

with controlled passband. There are examples of filters in the second case, which passband boundaries are changed tens of times [6],[10],[14]. Since the frequency response is function of the pole frequencies and Q-factors, which are tuned separately, additional specific tuning circuits are developed for complete tuning of the filter [6],[7],[11],[12].

Gyrator filters are one of the most often used classes of Gm-C filters. The capacitively loaded gyrator is equivalent to an inductor, which allows direct replacement of the cross (grounded) inductors in the LC ladder filters. The replacement of longitudinal (floating) inductors in the LC ladders requires more complicated circuit – two gyrators in cascade with cross capacitor between them [1],[2],[6]. The direct replacement of the inductors in the LC ladder filters preserves the most important advantage of these filters – their very low sensitivity concerning the element variations [1],[2]. However gyrator filters are not always designed in this way and often they are built by using of gyrator biquads derived from corresponding LC circuits [2]. Band-pass (BP) and low-pass (LP) sections are received from parallel LC circuit (Fig. 1(a) and (b)), while the high-pass section comes from the series LC tank (Fig. 1(c)). BP and LP sections have the same topology in fact and difference is in the place, where appears the output voltage. Gyrator based biquads are used for design of high order BP filters especially when more specific moving of their passband is necessary. Then the filters are designed as cascaded biquads [4],[5],[10], [17]-[20] or as equivalents of coupled LC filters [21].

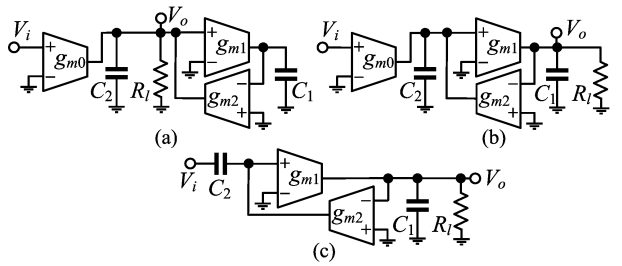

Fig. 1 BP (a), LP (b) and HP (c) second-order filters based on gyrator tank. The gyrator is formed by g_{m1} and g_{m2}, while g_{m0} converts the input voltage to an equivalent current, necessary for proper supplying the tank.

Therefore there is no big structural variety of the gyrator filters and the major efforts in their design are about the amplifiers in the gyrators. Practically all important filter parameters depend on gyrator OTAs. Transconductances together with used capacitors determine the frequency of operation. The range of g_m variation determines the filter tuning range. The OTA output impedances define the filter Q-factor and passband distortions of the frequency response. Very important is the linearization of the OTA and there are many papers describing different techniques for solving of this problem [9],[14],[15],[19]-[24]. Other problems in the design of gyrator filters are relating to the stabilizing of the dc operating points, minimizing of the noise. They are solved also during OTA design.

The goal of this paper is to investigate in more details a real circuit of fully differential gyrator BP biquad. The main focus is on the mutual dependence between the solutions of the different problems in the filter design: tunability, linearity, dc biasing and stabilization, etc. The second section considers briefly the basic properties of the gyrator simulated inductor and parallel gyrator tank; the third section is dedicated on the choice of the structure, design and simulation of appropriate OTA for the gyrator filter. The gyrator filter is described and investigated in the fourth section. All simulations are done with Cadence software for AMS 0.35 μm CMOS process used in the education [25].

2 Gyrator Simulated Inductors and Parallel Gyrator Resonance Circuit: Brief Review

The gyrator parallel resonance circuit is shown in Fig. 2(a) (the same as in Fig. 1(a) but without buffer amplifier). The OTA input and output parasitic capacitances are in parallel to C_1 and C_2 and are considered as parts of them. OTA input resistances are assumed infinitely high while their output resistances R_{o1} and R_{o2} are finite and in parallel to C_1 and C_2 respectively. The equivalent circuit of the gyrator simulated inductor is shown in Fig 2(b) [1],[2],[26] and its elements are

$$L = \frac{C_1}{g_{m1}g_{m2}}, \quad r = \frac{1}{R_{o1}g_{m1}g_{m2}}. \tag{1}$$

The frequency dependence of the Q-factor of the simulated inductance is [26]:

$$Q_L = \frac{2Q_m}{\omega/\omega_{Qm} + \omega_{Qm}/\omega}. \tag{2}$$

It has a maximum Q_m at frequency ω_{Qm}:

$$Q_m = \frac{g_{m1}g_{m1}R_{o1}R_{o2}}{2\sqrt{1+g_{m1}g_{m1}R_{o1}R_{o2}}} \approx \frac{1}{2}\sqrt{g_{m1}g_{m1}R_{o1}R_{o2}}; \tag{3}$$

$$\omega_{Qm} = \frac{1}{C_1}\sqrt{\frac{R_{o2}}{R_{o1}}g_{m1}g_{m2}}. \tag{4}$$

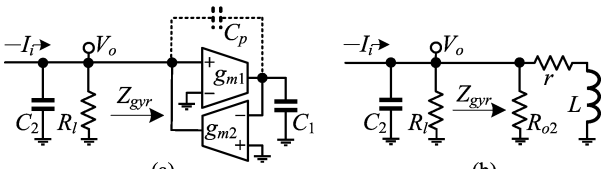

Fig. 2 (a) Gyrator parallel resonance circuit (C_p represents OTA parallel parasitic capacitance, existing in some cases); (b) its RLC equivalent circuit (without C_p).

Infinite load resistance is assumed in the analysis of the tank, which allows to reflect the effect of gyrator non-idealities on the properties. Tank resonance frequency usually is given by the formula

$$\omega_0 = \frac{1}{\sqrt{LC_2}} = \sqrt{\frac{g_{m1}g_{m2}}{C_1C_2}}, \quad (5)$$

which is valid if ideal OTAs with infinitely high output impedances are assumed. The resistors r and R_{o2} in Fig. 2(b) cause small deviation for real OTAs with limited output resistances and the following more strict formula can be derived for the real resonance frequency ω_{res}

$$\omega_{res} = \omega_0\sqrt{1+\frac{1}{4Q_m^2}}. \quad (6)$$

It should be used for small Q only – the error of formula (5) is less than 1% for $Q_m \geq 4$.

For the Q-factor of the resonance circuit is valid

$$\frac{1}{Q_{res}} = \frac{1}{\sqrt{4Q_m^2+1}}\left(\sqrt{\frac{C_1R_{o1}}{C_2R_{o2}}}+\sqrt{\frac{C_2R_{o2}}{C_1R_{o1}}}\right). \quad (7)$$

It is less or approximately equal to Q_m and the approximate equality is when $Q_m \geq 4$ and $C_1R_{o1} = C_2R_{o2}$. The last condition is in the case of equal capacitors and identical OTAs.

Another OTA imperfection, which affects the properties of the gyrator resonance circuit, is the limited OTA frequency bandwidth. Single pole approximation usually is used for the frequency response of the OTA's g_m [1],[6] and it causes increasing of the Q-factor according the formula [27]:

$$\frac{1}{Q_{res}'} \approx \frac{1}{Q_{res}} - 2\frac{\omega_{res}}{\omega_{gm}}, \quad (8)$$

derived under the assumption of identical OTAs. The parameters Q_{res} and ω_{res} are given by (6) and (7) (when g_m is frequency independent); and ω_{gm} is the pole frequency of g_m. This formula imposes stringent limitations about the frequency range of operation of the tank. For example, if Q_{res} = 10 and 10% deviation of its value is permitted, then ω_0 must be at least 200 times less than ω_{gm} [27].

The single pole approximation is more appropriate for multistage OTA. The frequency properties of a single stage differential OTA are defined basically by the capacitances of the amplifying transistors. Their gate-source capacitances are included in the OTA input capacitance; drain-source capacitances in the OTA output capacitance and gate-drain capacitances appear as additional capacitances between OTA input and output. In fact the small signal model for a single stage OTA is consisting of an amplifying core with no parasitic capacitances, and externally connected parasitic elements: capacitan-ces at the input and output; resistor at the output; and a transition capacitance between input and output. The transition capacitances of both OTAs in the single-ended gyrator model in Fig. 2(a) are combined in the capacitor C_p. The analysis of the circuit gives the following expressions for the changed resonance frequency and Q-factor:

$$\omega_{res}' = \omega_{res}/A, \quad (9)$$

$$\frac{1}{Q_{res}'} = \frac{1}{A}\left[\frac{1}{Q_{res}}+\frac{C_p}{\omega_{res}C_1C_2}\left(\frac{1}{R_{o1}}+\frac{1}{R_{o2}}+g_{m2}-g_{m1}\right)\right], \quad (10)$$

where A is the expression

$$A = \sqrt{1+\frac{C_p(C_1+C_2)}{C_1C_2}}. \quad (11)$$

The new resonance frequency ω_{res}' decreases relative to ω_{res}. The change of Q depends on the relationship between g_{m1} and g_{m2} – it can increase or decrease and even it can turn to negative (appearance of self-oscillation) if g_{m1} is enough high. In the most preferable case of identical OTA ($g_{m1} = g_{m2}$) the circuit is stable and $Q_{res}' < Q_{res}$.

Another requirement in the design of the resonance circuit is the equality of the maxima of the voltages at the OTA outputs – it is necessary for optimal dynamic range of the circuit [1]. The analysis of this requirement leads to the following condition

$$C_1/C_2 \approx g_{m1}/g_{m2}, \quad (12)$$

which usually is satisfied as two equalities $C_1 = C_2$ and $g_{m1} = g_{m2}$ (again identical OTAs and equal capacitors).

The short review of the properties of the gyrator tank presented in this section shows that the identity of gyrator OTAs as well equality of its both capacitors is highly desirable, suggesting several important benefits. This identity is achieved easier in the case of differential OTAs – then the negative g_m of the second OTA is realized as appropriate connection of the OTA input and output terminals.

3 Amplifiers Forming the Gyrator

3.1 Basic Circuit of the OTA

In accordance to the conclusion in the previous section the gyrator, considered here, consists of identical amplifiers. Their circuits are based on the OTA shown in Fig. 3. This is single stage fully differential amplifier with dynamic load (transistors M_7 and M_8) and source degeneration. The common-mode feedback (CMFB) circuit, necessary for stabilizing the dc output voltage, is also shown in Fig. 3. This circuit is very similar to those presented in [9] with some small modifications.

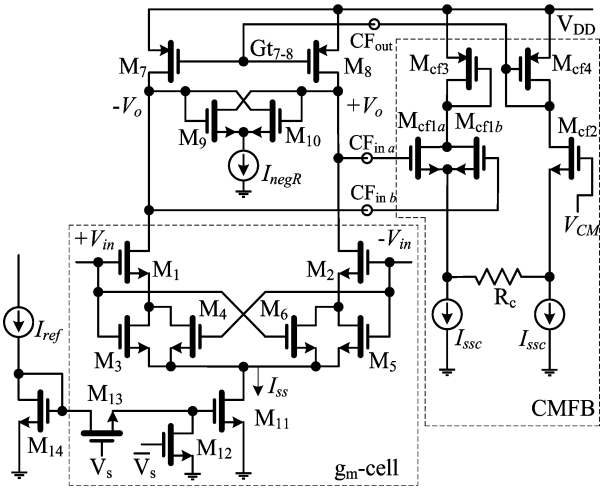

Fig. 3 OTA used for forming the gyrator.

For increasing the Q-factor of the tank a negative resistance created by the pair M_9-M_{10} is added in parallel to the OTA output. This approach is preferred due to some its benefits. Formula (3) shows that Q can be increased by increasing of OTA g_m or by increasing of their output resistances. However the use of transconductances is not convenient due to: 1) Higher g_m often requires amplifier with more than one stage, which decreases its pole frequency. 2) OTA g_ms determine also the resonance frequency of the tank and their simultaneously use for increasing of Q makes difficult the tuning of the filter. The negative resistance created by M_9-M_{10} in Fig. 3 is controlled by the current source I_{negR} and allows independent control of OTA output resistance.

The source degeneration of the main differential pair M_1 and M_2 is proposed in [28]. It is dynamic and consists of two pairs M_3-M_4 and M_5-M_6 in the sources of M_1 and M_2. They operate in linear region and the cross-connection of the gates as is shown in Fig. 3 gives better improving the linearity. A benefit of this circuit is preserving of the frequency range of the amplifier [28].

According [9], OTA linearization depends on the relationship between the sizes of the transistors M_1 and M_2 in the main differential pair and of the degeneration transistors M_3-M_6. The following parameter is introduced as a criterion for this relationship

$$a = \frac{(W/L)|_{M1-M2}}{(W/L)|_{M3-M6}} \tag{13}$$

and a = 2 is recommended in [9] as optimal. However this value is questionable since there is no clear criterion about linearity. Here will be used total harmonic distortion (THD) of the ac output current at short circuited output (between points $-V_o$ and $+V_o$ in Fig. 3) and the range of the amplitudes of the input voltage, at which THD is under some limit. This limit is defined from the behavior of the gyrator tank when OTAs have weak nonlinearity. An approximate consideration done in [29] shows that when Q is high (above 20) even THD of 0.5% causes visible distortion of the frequency response and change of the resonance frequency.

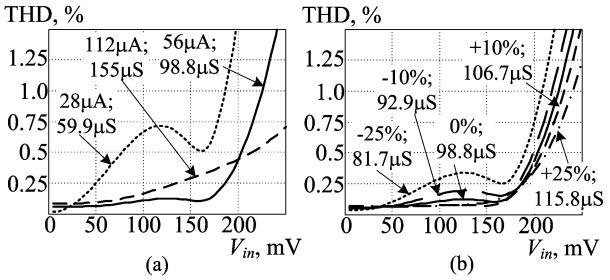

Fig. 4 THD of the OTA output current vs. input voltage amplitude: (a) At three significantly different values of the tail current I_{ss} (for each curve are given the corresponding values of I_{ss} and g_m). (b) At relatively small deviation I_{ss} from 56μA (the percentage deviation from I_{ss} and g_m are given for each curve).

More detailed investigation based on this criterion however shows the optimal a depends from the absolute sizes of the transistors as well from the dc currents through the transistors. This is illustrated in Fig. 4(a). The OTA is designed initially for g_m = 100μS, which is achieved at tail current I_{ss} = 56μA (the current through M_{11}). The sizes of the transistors are $W_{M1\text{-}M2}$ = 16μm; $W_{M3\text{-}M6}$ = 8μm and for all these transistors L = 0.35μm. At these conditions the optimal value for a is a = 2. When I_{ss} is increased and decreased twice, the corresponding curves in Fig. 4(a) demonstrate a deviation from the optimality: from THD < 0.25% for input amplitudes up to 180 mV at I_{ss} = 56μA to THD up to 0.75% for the same range of the input amplitudes when I_{ss} = 28μA. By varying of the widths of M_3-M_6 at I_{ss} = 28μA is determined new optimal a to about 1.6 – 1.7, having as criterion the widest input voltage range, at which THD < 0.25%.

Of course, smaller changes of I_{ss} cause less changes in the linearity. This is illustrated in Fig.

4(b) for the considered case where is shown how changes THD when I_{ss} varies within ±25% from the initial value of 56µA – only the curve for -25% differs more significantly.

3.2. OTA with Programmable g_m

The last consideration in the previous subsection shows that the method for tuning of the filter by changing of the tail currents of the OTA cannot give wide tuning range if the circuit in Fig. 3 is used, since large variation of I_{ss} causes also a significant reducing of the permitted input voltage. For this reason a different approach is chosen for widening of the tuning range. Every OTA in the gyrator consists of three different g_m-cells with g_ms equal to 50µS, 100µS and 200µS, which inputs and outputs are connected in parallel (Fig. 5). Each cell can be switched on and off by controlling voltages V_s and $\overline{V}_s$, having opposite values (low-high or high-low). They control two switches in the g_m-cell (M_{12} and M_{13} in Fig. 3), which allow or stop the tail current in the cell. In fact only one of the voltages V_s and $\overline{V}_s$ is enough for switching the cell – the other voltage can be produced by an inverter. In this way can be achieved 7 different g_ms from 50µS till 350µS in steps of 50µS. If continuous tuning is needed then this approach can be combined with varying of the tail currents in the g_m-cells. But now the variation is small (less that 10-15%) and will not deteriorate significantly the dynamic range.

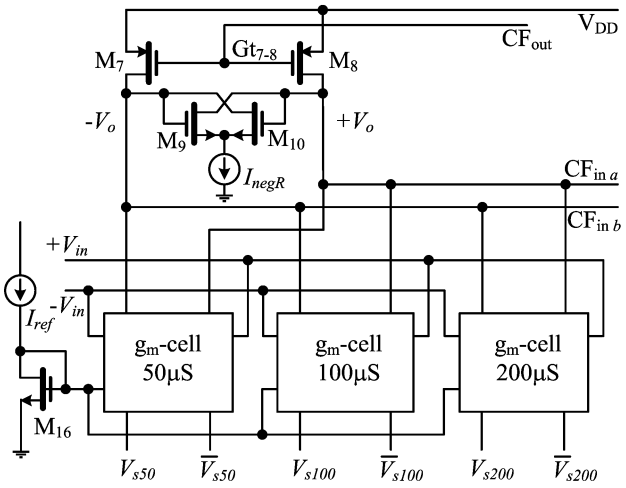

Fig. 5 Block-diagram of OTA consisting of three g_m-cells.

The complete circuit of the OTA is shown in Fig. 5 (CMFB circuit is not shown there). Except the main terminals for the signal ($+V_{in}$, $-V_{in}$ for input and $+V_o$, $-V_o$ for output) OTA has several additional controlling terminals: V_s and $\overline{V}_s$ for all g_m-cells; $CF_{in\,a}$ and $CF_{in\,b}$ to CMFB input; CF_{out} from CMFB output; terminal for the reference current of the tail currents in the g_m-cells; and terminal for controlling the current I_{negR}.

The g_m-cells in this circuit are partly optimized by varying of the transistors sizes and the tail currents in order to have approximately equal ranges of the differential input voltage, in which THD of the output current (at short circuited output) is low – 0.25% or less. The result for the width/length in µm for the transistors in the cells and for their tail currents are given in Table 1.

Table 1. Sizes of the transistors (in µm) and of the tail currents in the g_m-cells

Cell	W/L (M_1-M_2) µm	W/L (M_3-M_6) µm	W/L (M_{11}) µm	I_{ss} µA
50µS	8/0.35	4/0.35	7/0.35	28
100µS	16/0.35	8/0.35	14/0.35	56
200µS	30/0.35	15/0.35	30/0.35	120

The other transistors in Fig. 3 and Fig. 5 have the following sizes (W/L) in µm: M_7-M_8 – 40/0.35; M_9-M_{10} – 0.65/0.5; M_{16} – 15/0.35; M_{cf1a} and M_{cf1b} – 5/0.35; M_{cf2}-M_{cf4} – 10/0.35. The reference current is I_{ref} is 55µA. The supply voltage is 3.3V. In all simulations bellow the dc voltages at the OTA inputs $+V_{in}$ and $-V_{in}$ is fixed at 2.2V. The voltages at the outputs $+V_o$ and $-V_o$ is kept by CMFB approximately the same, which is achieved when V_{CM} = 2.1V.

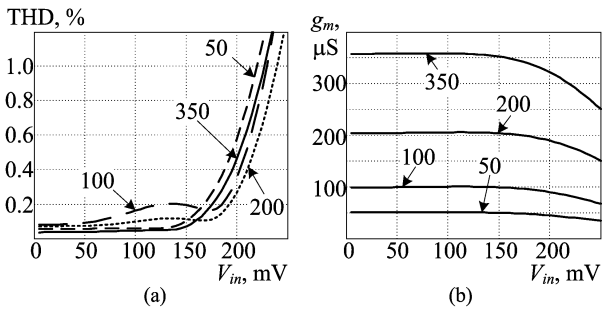

Fig. 6 (a) THD of the output current vs. amplitude V_{in} of the input voltage when different OTA cells are switched on; (b) approximate dependence of g_m from V_{in} when different OTA cells are switched on.

The dependence of the nonlinear distortion of the ac output current from the amplitude of the input voltage is illustrated in Fig. 6. It shows THD vs. V_{in} and g_m vs. V_{in} for each cell separately and when all cells are connected in parallel (g_m = 350µS). The simulations are done at relatively low frequency of 10kHz, when the OTA parasitic capacitances have no effect. The short circuit at the output is realized by a capacitor of 10nF and the circuit for negative resistance at the output is switched off by setting I_{negR} = 0. The curves confirm that all cells keep their linearity (THD ≤ 0.25-0.3%) in approximately same range of the input voltage.

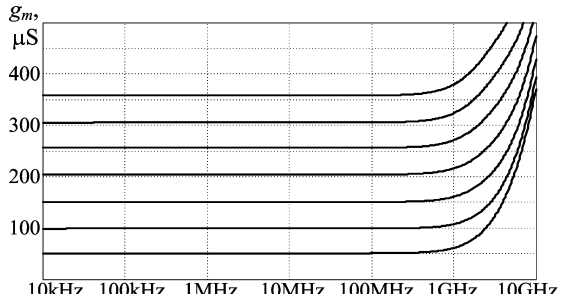

Fig. 7 Frequency responses of g_m, when OTA is adjusted to g_m = 50, 100, 150, 200, 250, 300, and 350 μS.

The frequency properties of the OTA are illustrated in Fig. 7, where are given the frequency dependences of g_m for all possible combination of cells. All curves increase above certain frequency in the range between 500MHz and 1GHz. This increasing confirms the model with a transition capacitance between input and output for single stage OTAs used in Section II. Since the output is short circuited when g_m is simulated, the transition capacitance at high frequency transfers additional current from the voltage source at the input to the short circuit at the output, where g_m is measured.

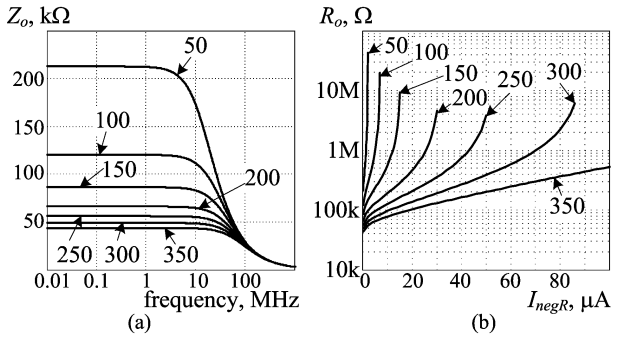

Fig. 8 Simulation of OTA output impedance: (a) frequency response; (b) dependence from the current I_{negR}, controlling the negative resistance. For each curve is given the corresponding OTA transconductance in μS.

Another important OTA parameter is its output resistance R_o defining Q of the tank, when no negative resistances are used. The frequency dependences of output impedances for each value of g_m are given in Fig. 8(a) and the output resistances are the low frequency values of the impedances. As it is expected, R_o is smaller when g_m is bigger. The output resistance of one g_m-cell is

$$R_o \approx (r_{o\,M1} + r_{o\,M2}) || (r_{o\,M7} + r_{o\,M8}). \quad (14)$$

In this formula $r_{o\,M1}$, $r_{o\,M2}$, $r_{o\,M7}$ and $r_{o\,M8}$ are drain-source resistances in the small-signal models of the corresponding transistors, given by the approximate formula [30]

$$r_o \approx 1/(\lambda I_D), \quad (15)$$

where λ is the slope of the VA characteristic in saturation and I_D is dc drain current through the transistor. Cells with higher g_ms work at higher dc drain currents in the differential pairs, which makes r_o of the transistors smaller and reduces the total R_o of the OTA.

Fig. 8(b) shows how R_o changes from the current I_{negR}. The negative conductance emulated by the pair M_9-M_{10} is [30]

$$G_{M9-M10} = -g_m/2 = -\sqrt{\frac{1}{2}\mu_n C_{ox}\frac{W}{L} I_D}, \quad (16)$$

where g_m is the transconductance, μ_n is the mobility, C_{ox} is gate-oxide capacitance per unit area – all these parameters together with W, L and I_D are for one of M_9 or M_{10}. When I_{negR} increases the magnitude of $G_{M9\text{-}M10}$ also increases and reduces the total OTA output conductance. The curves in Fig. 8(b) are given for the range of I_{negR}, in which OTA output resistance is still positive. They show that R_o can be controlled effectively by I_{negR} for smaller values of OTA transconductance. When OTA g_m is 350μS, R_o increases slowly and cannot be turned to negative at all. The reason is: The current I_{negR} flows through dynamic loads M_7 and M_8 and its increasing causes increasing of their output conductance ($1/r_o$). This effect is small when I_{negR} is significantly small than the tail current I_{ss}. When both currents are of the same range then the increasing of the negative conductance emulated by M_9-M_{10} cannot compensate completely the increasing of output conductances of M_7 and M_8. This effect can be avoided by applying particular circuits for negative resistance in each g_m-cells. They can be designed to operate at relatively small currents I_{negR} by proper choice of the ratio W/L in MOSFETs.

3.3 Common-Mode Feedback Circuit

CMFB circuit is given in Fig. 3. It is realized as degenerated differential stage with split tail current source [30]. OTA output dc voltages (at points $+V_o$ and $-V_o$ in Fig. 3) are sensed by the parallel transistors M_{cf1a} and M_{cf1b}, which complete current is proportional to the averaged OTA dc output voltages. CMFB is investigated at the beginning of all simulations aiming to determine some of its components and to prove its stabilizing effect on OTA output dc voltage as well its ac stability. First is determined the value of the currents I_{ssc} of the current mirrors in CMFB circuit. Fig. 9(a) shows how this current affects the dc voltage $V_{o\,dc}$ at OTA outputs. Evidently there is a minimum value of this current in the range of 5-15μA, which depends on the reference

voltage V_{CM}. The value of I_{ssc} should be far from this minimum in order to ensure secure operation of the CMFB. The next simulation, investigating how CMFB stabilizes OTA output dc voltage against the variation of the OTA input dc voltage, is done at I_{scc} = 20, 30 40 and 60μA. The plot in Fig. 9(b) shows that CMFB works well at all values of I_{ssc}: total variation of $V_{o\,dc}$ of about 50mV when the voltage at the input changes from 1 to 3.3V. In all other simulations I_{scc} = 40μA – a value, which probably is a bit bigger than necessary, however it is chosen to avoid possible problems caused by incorrect work of CMFB.

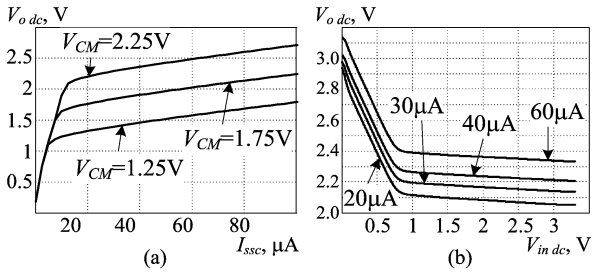

Fig. 9 Dc simulation of CMFB: (a) dc voltage at OTA outputs vs. currents I_{ssc}; (b) dc voltage at OTA outputs vs. dc voltage at OTA inputs at different values of I_{ssc} and V_{CM} = 2.1V.

The simulations in Fig. 9 are for OTA in which all g_m-cells are on. The switching the cells on and off also affects the output dc voltage and its total variation is about 0.2V when OTA g_m changes from 50μS to 350μS. However this variation can be compensated by proper change of V_{CM} simultaneously with the switching of the cells.

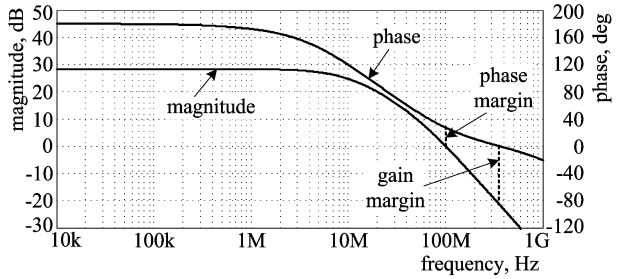

Fig. 10 Frequency response (magnitude and phase) of the open loop gain of CMFB.

Another investigation is about ac stability of CMFB which is done by simulating the gain through the feedback loop when this loop is open. The plot in Fig. 10 shows a phase margin of about 30° and a gain margin of about 20dB.

4 The Gyrator Resonance Circuit and Its Properties

A detailed block-diagram of the gyrator tank is shown in Fig. 11. It is fully differential version of the basic circuit in Fig. 1(a) with included controlling signals and CMFB block. The gyrator is formed by OTA 1 and OTA 2. They are identical and every one of them is according to Fig. 5. At the input is placed another amplifier – OTA 0, which works as buffer, converting the input voltage to an equivalent current, necessary for proper operation of the tank. It is not object of the investigation and it is replaced in the simulations by ideal voltage-controlled current source (VCCS).

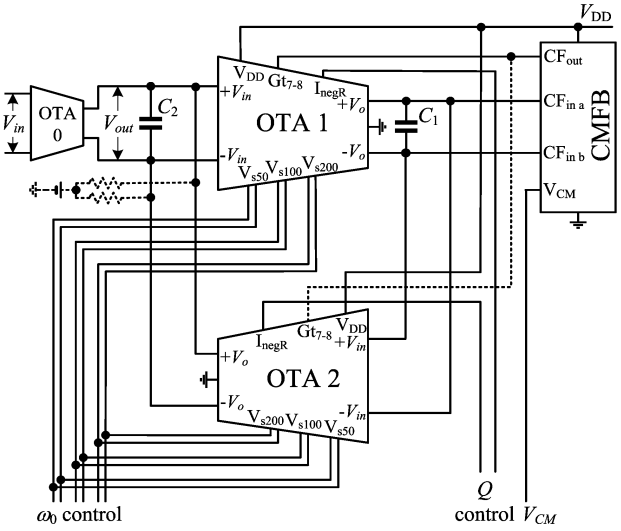

Fig. 11 Block-diagram of the gyrator resonance circuit.

CMFB circuit controls only the output dc voltages of OTA 1. The output of OTA 2 is in parallel to the output of OTA 0 (or another circuit ensuring the proper operating conditions at the gyrator input) and in the reality its output dc voltage is defined by OTA 0. Since OTA 0 is replaced by ideal VCCS in the simulations presented here, dc output voltage of OTA 2 is defined by an artificial way – by a dc voltage source connected to the outputs through large resistors (> 1GΩ). The dc gate voltage of the transistors M_7 and M_8 for this OTA is taken from the CMFB of OTA 1. All these connections are shown by dotted lines in Fig. 11.

The switching of g_m-cells in both OTAs and tuning in this way the resonance frequency is by the same control signals, keeping the OTA g_ms always equal. On the other hand the tuning of Q by the negative resistances at OTA outputs is by two independent lines connected to terminals I_{negR} because the resistors, which appear in parallel at both gyrator outputs, could be different.

The output voltage V_{out} is taken in parallel to C_2 as it is shown in Fig. 11 and the circuit is fully differential equivalent of the bandpass biquad in Fig. 1(a). Strictly speaking it differs slightly from the bandpass filter since its transfer function is

$$H(s) = \frac{V_{out}}{V_{in}} = \frac{h(s+z)}{s^2+\frac{\omega_{res}}{Q_{res}}s+\omega_{res}^2}, \quad (17)$$

where ω_{res} and Q_{res} are given by (6) and (7) correspondingly. The zero z introducing the deviation from the standard banpass transfer function is due to the limited output resistance of OTA 1 and is equal to $1/(R_{o1}C_1)$. The ratio z/ω_0 is

$$\frac{z}{\omega_0} = \frac{1}{2Q_m}\sqrt{\frac{C_2R_{o2}}{C_1R_{o1}}}. \quad (18)$$

When Q_m is high the zero is at a frequency much less than the resonance frequency and has no significant effect on the frequency response. The parameter h is equal to g_{m0}/C_2 and it determines the gain at the resonance frequency

$$|H(j\omega_{res})| = \frac{g_{m0}R_{o2}}{1+\frac{C_2R_{o2}}{C_1R_{o1}}}. \quad (19)$$

It seems from this formula that $|H(j\omega_{res})|$ does not changes when the filter is tuned by changing the g_ms of the gyrator OTAs. However this is not true, since the switching of the g_m-cells changes also the OTA output impedance and the change of the gain at ω_{res} should be compensated by a proper change of g_{m0}.

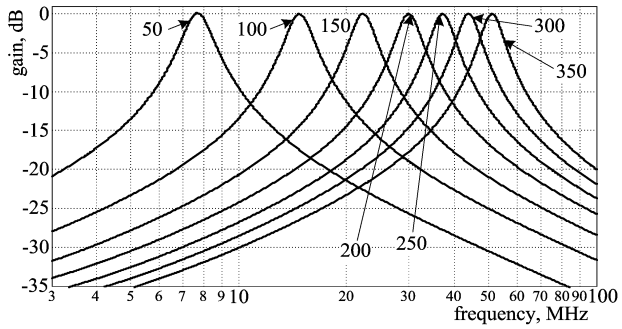

Fig. 12 Frequency responses of the gyrator bandpass filter at different values of OTA g_ms and without Q boosting.

The frequency responses (linear analysis) of the filter are simulated for all possible values for the OTA g_ms from 50μS to 350μS. This is done for two cases: 1) When there is no Q-boosting by the negative resistances at the OTA outputs (I_{negR} = 0); 2) When Q is increased approximately to 40 by corresponding increasing of I_{negR}. The plots are given in Fig. 12 and Fig. 13 respectively. For better comparison of the curves, g_{m0} is adjusted together with g_{m1} and g_{m2} in order to have 0dB gain at the frequency of the maximum. The basic data for the frequency responses extracted from the simulations are summarized in Table 2. It could be underlined the very small dependence of the resonance frequency, when the Q-factor is tuned by the negative resistances.

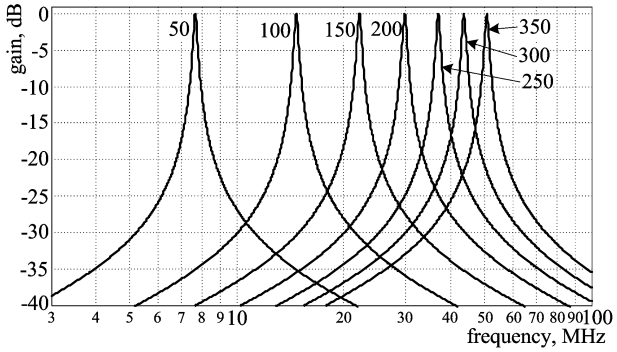

Fig. 13 Frequency responses of the gyrator bandpass filter at different values of OTA g_ms and when Q is boosted to approximately 40.

Table 2. Parameter of the filter frequency responses

	OTA g_m	50μS	100μS	150μS	200μS	250μS	300μS	350μS
no Q boosting	f_{res}, MHz	7.678	14.79	22.25	29.91	37.20	43.97	51.10
	Q	5.3	5.8	6.2	6.35	6.55	6.7	6.9
	g_{m0}, μS	9.89	17.66	24.95	32.85	39.45	46.81	52.42
Q≈40	f_{res}, MHz	7.641	14.74	22.17	29.76	37.02	43.76	50.73
	g_{m0}, μS	1.3	2.5	3.9	5.24	6.4	7.52	8.84

The effect of the OTA nonlinearity on the frequency response of the gyrator tank is studied for two cases: when OTA g_ms are equal to 200μS and when they are 350μS. In both cases Q of the filter is approximately 20. At the beginning of the investigation is performed frequency analysis, when the desired Q is adjusted by varying of I_{negR} and also is determined the frequency f_{res} (= $\omega_{res}/(2\pi)$) of maximum of the frequency response. Then a sinusoidal voltage source for time domain analysis is applied at the filter input and its magnitude V_{in} is adjusted in order to have the desired magnitude of the voltage V_{out} (the voltage at the input of the gyrator tank) at frequency f_{res}. The frequency response is received by determining the steady-state magnitude of V_{out} at different frequencies, keeping V_{in} unchanged.

The frequency responses are given in Fig. 14. The parameter there, defining different curves, is the magnitude of V_{out} at f_{res}. The curves represent the normalized gain, i.e. the gain divided by its maximum value at f_{res}. This mode allows to see better the distortion of the frequency response at the higher signal, however it hides the gain compression effect. Except the gain at different magnitudes of V_{out}, for comparison is given the linear case (marked as "li-

near"), i.e. the response received by frequency domain simulation.

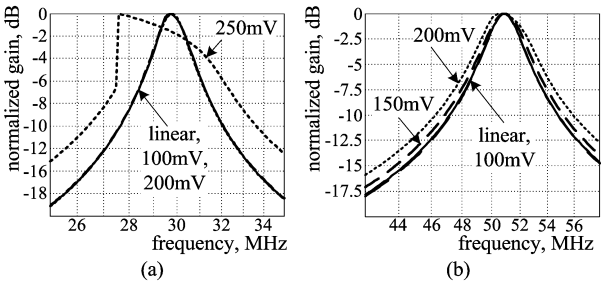

Fig. 14 Normalized gain of the gyrator filter vs. frequency at different magnitudes of the output voltage V_{out} of the filter and $Q \approx 20$: (a) When OTA g_ms are equal to 200μS; (b) When OTA g_ms are equal to 350μS.

Fig. 14(a) shows that the filter at g_m = 200μS is practically linear up to 200mV magnitude of V_{out} and above it appears nonlinearity, expressing in appearance of "jump phenomenon" [29] in the curve for 250mV. Looking in Fig. 6(a), it is easy to see the explanation: THD at g_m = 200μS is less than 0.3% for OTA input voltages below 200mV and increases to 1.2% at 250mV. Different is the behavior of the curves in Fig. 14(b) – the filter is linear to magnitudes of 100mV. For magnitudes to 200mV the nonlinear effects express as decreasing of the Q-factor (wider curve) and above this voltage appears trend for distortion of the frequency response. THD of the OTA as also small – below 0.1% for voltages less than 150mV and 0.5% at 200mV. The reason for this behavior of the filter in this case is the OTA output resistance – the desired Q is received at high value of the current I_{negR} and the nonlinearity of the transconductances of the transistors M_9 and M_{10} has significant effect.

Gain compression is observed also. Compared with the gain at the lowest output magnitude of 100mV at f_{res}, the gains at the frequency of the maximum decrease with increasing of the output magnitude as follows: when g_m = 200μS by 0.39dB at 200mV and by 2.49dB at 250mV; when g_m = 350μS by 0.46dB at 150mV and by 1.34dB at 200mV.

5 Conclusion

A fully differential gyrator resonance circuit with tunable resonance frequency is designed and partly optimized. The focus of the considerations is on the problems, which appear when wide frequency tuning range is needed, and on the ways for their overcoming. The gyrator consists of identical single-stage OTAs with source degeneration for improving the linearity and theoretically is proved that OTA identity is significant requirement in this case in order to avoid instability of considerable decreasing of the Q-factor. The amplifiers consist of three different differential stages, having g_m of 50, 100 and 200μS, which can be switched on and off independently by control of their tail currents. They are connected in parallel and the total g_m of the amplifier can be switched in this way from 50μS to 350μS in steps of 50μS. This approach for tuning the OTA g_m is chosen in order to preserve approximately the same range of linear operation for all frequencies, at which the gyrator filter will be tuned. The designed OTA is investigated by computer simulation in order to characterize its most important parameters – g_m, output impedance, their frequency response, CMFB and its properties.

The realized and simulated gyrator filter can be tuned from 7.68MHz to 51.1MHz. This tuning range can be extended by adding more parallel g_m-cells in the amplifiers. The Q factor is also tunable by using of negative resistances in parallel to gyrator outputs and this tuning is independent from the tuning of its frequency. Of course, the filter is not completely optimized concerning all its parameters, however the paper marks some of the basic problems, which appear in the design of gyrator filters and proposes possible solutions for them.

Acknowledgement

This work was supported by contract DUNK 01/03-12.2009 funded by National Science Fund of the Ministry of Education, Youth and Science of Bulgaria.

References

[1] T. Deliyannis, Y. Sun, J. K. Fidler, *Continuous-Time Active Filter Design*, CRC Press, 1999.

[2] R. Schaumann, M. E. Van Valkenburg, *Design of Analog Filters*, Oxford University Press, 2001.

[3] V. Agarval, S. Sonkusale, Ultra low-power PVT independent sub-threshold gm-C filters for low-frequency biomedical applications, *Analog Integrated Circuits and Signal Processing*, 2011, vol. 66, pp. 285-291.

[4] A. Veeravalli, E. Sanchez-Sinencio, J. Silva-Martinez, A CMOS Transconductance Architecture With Wide Tuning Range for Very Low Frequency Applications, *IEEE Journal of Solid-State Circuits*, vol. 37, No. 6, pp. 776-781, June 2002.

[5] S. Ren, C. Benedik, RF CMOS active inductor band pass filter with post fabrication calibration, *Int. Journal of Electronics and Communications (AEÜ)*, 67(2013), pp. 1058-1067.

[6] Y. Sun, ed., *Design of High Frequency Analog Integrated Filters*, The Institutions of Electrical Engineers, 2002.

[7] A. Karsilayan, R. Schaumann, Mixed-mode automatic tuning scheme for high-Q continuous time filters, *IEE Proceedings – Circuits, Devices and Systems*, vol. 147, No. 1, pp. 57-64, Feb. 2000.

[8] C. Hung, K. Halonen, M. Ismail, V. Porra, Micropower CMOS Gm-C Filters For Speech Signal Processing, *1997 IEEE Int. Symp. Circuits and Systems (ISCAS 1997)*, Hong-Kong, June 12-14, 1997, pp. 1972-1975.

[9] Y. Sun, C. J. Jeong, I. Y. Lee, J. S. Lee, S. G. Lee, A 50-300 MHz Low Power and High Linear Active RF Tracking Filter for Digital TV Tuner ICs, *Proc. 2010 IEEE Custom Integrated Circuits Conf. (CICC 2010)*, San Jose, USA, 19-22 Sept. 2010.

[10] A. Tajalli, Y. Leblebici, Low-Power and Widely Tunable linearized Biquadratic Low-Pass Transconductor-C Filter, *IEEE Trans. Circuits and Systems – II: Express Briefs*, vol. 58, No. 3, pp. 159-163, March 2011.

[11] F. Behbahani, W. Tan, A. Karimi-Sanjaani, A. Roithmeier, A. Abidi, A Broad-Band Tunable CMOS Channel-Select Filter for a Low-IF Wireless Receiver, *IEEE Journal of Solid-State Circuits*, vol. 35, No. 4, pp. 476-489, April 2000.

[12] J. F. Fernandez-Bootello, M. Delgado-Restituto, A. Rodriguez-Vazquez, A 0.18 µm CMOS Low-Noise Elliptic Low-Pass Continuous-Time Filter, *2005 IEEE Int. Symp. Circuits and Systems (ISCAS 2005)*, May 23-26, 2005, Kobe, Japan, pp. 800-803.

[13] A. Otin, C. Aldea, S. Celma, Low-Voltage LC Ladder Gm-C Low-Pass Filters With 42-215 MHz Tunable Range, *2005 European Conf. on Circuit Theory and Design*, Aug. 29-Sept. 1, 2005, Cork, Ireland, vol. 1, pp. 245-248.

[14] P. Crombez, J. Craninckx, P. Wambacq, M. Steyaert, A 100 kHz to 20 MHz Reconfigurable Power Linearity Optimized Gm-C Biquad in 0.13 µm CMOS, *IEEE Trans. Circuits and Systems – II: Express Briefs*, vol. 55, No. 3, pp. 224-228, March 2008.

[15] K. Kwon, A 50- to 300 MHz CMOS Gm-C Tracking Filter Based on Parallel Operation of Saturation and Triode Transconductors for Digital TV Tuner ICs, *IEEE Trans. Circuits and Systems – II: Express Briefs*, vol. 62, No. 6, pp. 522-526, June 2015.

[16] S. Pavan, Y. Tsividis, Time Scaled Electrical Networks – Properties and Application in the Design of Programmable Analog Filters, *IEEE Trans. Circuits and Systems – II: Analog and Digital Signal Processing*, vol. 47, No. 2, pp. 161-165, Feb. 2000.

[17] P. Pandey, J. Silva-Martinez, X. Liu, A CMOS 140-mW Fourth-Order Continuous-Time Low-Pass Filter Stabilized With a Class-AB Common-Mode Feedback Operating at 550 MHz, *IEEE Trans. Circuits and Systems – I: Regular Papers*, vol. 53, No. 4, pp. 811-820, April 2006.

[18] C. Duan, W. Li, A 46 MHz Biquad Gm-C High Q Bandpass Filter Design for Wireless Application, *2011 IEEE 9th Int. Conf. on Dependable, Autonomic and Secure Computing*, Dec. 12-14, 2011, Sidney, Australia, pp. 70-72.

[19] T.-Y. Lo, C.-L. Kuo, C.-C. Hung, Negative current feedback OTA with application to 250 MHz Gm-C filter, *Analog Integrated Circuits and Signal Processing*, 2012, vol. 73, pp. 123-129.

[20] S. Hori, N. Matsuno, T. Maeda, H. Hida, Low-Power Widely Tunable Gm-C Filter Employing an Adaptive DC-blocking, Triode-Biased MOSFET Transconductor, *IEEE Trans. Circuits and Systems – I: Regular Papers*, vol. 61, No. 1, pp. 37-47, Jan. 2014.

[21] H. L.-Thai, H.-H. Nguyen, H.-N. Nguyen, H.-S. Cho, H.-S. Lee, S.-G. Lee, An IF Bandpass Filter Based on Low Distortion Transconductor, *IEEE Journal of Solid-State Circuits*, vol. 45, No. 11, pp. 2250-2261, Nov. 2010.

[22] E. Sanchez-Sinencio, J. Silva-Martinez, CMOS transconductance amplifiers, architectures, and active filters: a tutorial, *IEE Proceedings – Circuits, Devices and Systems*, vol. 147, No. 1, pp. 3-12, Feb. 2000.

[23] A. Lewinski, J. Silva Martinez, OTA Linearity Enhancement Technique for High Frequency Applications with IM3 Below -65 dB, *IEEE Trans. Circuits and Systems – II: Analog and Digital Signal Processing*, vol. 51, No. 10, pp. 542-548, Oct. 2004.

[24] S. Ouzounov, E. Roza, H. Hegt, G. v.d. Veide, A. van Roermund, Design of MOS transconductance with low noise and low harmonic distortion for minimum current consumption, *INTEGRATION, the VLSI journal*, 40(2007), pp.365-379.

[25] Austriamicrosystems, "0.35 µm CMOS 50V Process Parameters", Eng-238, revision 4.0, December 2005.

[26] G. S. Moschytz, *Linear Integrated Networks - Fundamentals*, Van Nostrand Reinholds Co., 1974.

[27] H. Voorman, H. Veenstra, Tunable High-Frequency *Gm-C* filters, *IEEE Journal of Solid-State Circuits*, vol. 35, No. 8, pp. 1097-1108, Aug. 2000.

[28] V. Prodanov, G. Palaskas, J. Glas, V. Boccuzzi, A CMOS AGC-less IF .Strip for Bluetooth, *Proceedings of the 27th European Solid-State Circuit Conference (ESSCIRC 2001)*, Sept. 2001, pp. 490-493.

[29] A. Tanev, I. Uzunov, M. Hristov, S. Ouzounov, Study of Nonlinear Effects in Parallel Gyrator Resonance Circuit, *51st International Scientific Conference on Information, Communication and Energy Systems and Technologies "ICEST 2016"*, June 29-30, Ohrid, Macedonia.

[30] B. Razavi, *Design of CMOS Integrated Circuits*, 2nd ed., Mc Grow Hill, 2016.